Dynamics of Tethered Payloads with Deployment Rate Control

Arun K. Banerjee*
Lockheed Missiles & Space Company, Sunnyvale, California 94089

Introduction

DYNAMICS of deployment of a tethered payload from an orbiting spacecraft has been studied by both lumped mass and continuum models.[1-3] Although both models have advantages and disadvantages, the lumped-mass model is believed to be more general in that it describes small curvature and large elastic displacement of the tether. On the issue of control, both tether tension control[5] and tether deployment rate control[4,6] have been proposed, though deployment rate control is definitely easier to mechanize. A theory for deployment rate control with a lumped-mass model of the tether has not been published in the literature, to the best of the author's knowledge. The present Note seeks to fill this void.

Model Description

The model is shown in Fig. 1, where spacecraft B is a rigid body. The tether is represented by a variable number n of spring-connected lumped-mass particles; the tether length is equally divided into $n_{\max}$ number of segments when the tether is fully deployed, with the mass of each segment lumped in halves at its ends. The payload itself is a particle such that its mass together with half the mass of a tether segment forms mass m_1. In essence, this is the model used in Ref. 1. Point E represents the Earth and is assumed to be inertially fixed. Let $\boldsymbol{b}_1$, $\boldsymbol{b}_2$, $\boldsymbol{b}_3$ denote unit vectors fixed in B.

Kane's method[7] of deriving equations, which is used in this Note, allows flexibility in the choice of generalized speeds that describe the motion. These generalized speeds are chosen to simplify the equations of motion and can be introduced without even introducing the generalized coordinates.[8] The following choice of generalized speeds yields particularly simple dynamical equations for the system under consideration.

$$u_i = \boldsymbol{\omega}^B \cdot \boldsymbol{b}_i \qquad (i = 1,2,3) \tag{1a}$$

$$u_{3+i} = \boldsymbol{v}^C \cdot \boldsymbol{b}_i \qquad (i = 1,2,3) \tag{1b}$$

$$u_{3+3j+i} = \boldsymbol{v}^{P_j} \cdot \boldsymbol{b}_i \qquad (i = 1,2,3;\ j = 1,\ldots, n) \tag{1c}$$

where $\boldsymbol{\omega}^B$ is the angular velocity of B, $\boldsymbol{v}^C$ the velocity of C (the mass center of B), and $\boldsymbol{v}^{P_j}$ the velocity of P_j, the jth lumped mass. The configuration variables are defined by the following generalized coordinates (see Fig. 1), rather than by the inertial coordinates of Ref. 1, for computational accuracy.

$$q_{3j-3+i} = \boldsymbol{p}^{P_0P_j} \cdot \boldsymbol{b}_i \qquad (i = 1,2,3;\ j = 1,\ldots, n) \tag{2a}$$

$$q_{3n+i} = \boldsymbol{p}^{EC} \cdot \boldsymbol{b}_i \qquad (i = 1,2,3) \tag{2b}$$

where $\boldsymbol{p}^{PP}$ is the vector from P_0 to P_j, and $\boldsymbol{p}^{EC}$ is the vector from E to C. The tether exits the spacecraft at point P_0, given by the offset components

$$p_i = \boldsymbol{p}^{CP_0} \cdot \boldsymbol{b}_i \qquad (i = 1,2,3) \tag{3}$$

Received Dec. 5, 1988; revision received March 23, 1989.

*Senior Staff Engineer.

Kinematical Equations

The angular velocity of B and the velocities of C and P_j follow from Eqs. (1).

$$\boldsymbol{\omega}^B = \sum_{i=1}^{3} u_i \boldsymbol{b}_i \tag{4a}$$

$$\boldsymbol{v}^C = \sum_{i=1}^{3} u_{3+i} \boldsymbol{b}_i \tag{4b}$$

$$\boldsymbol{v}^{P_j} = \sum_{i=1}^{3} u_{3+3j+i} \boldsymbol{b}_i \qquad (j = 1,\ldots, n) \tag{4c}$$

Note that the preceding angular velocity and velocity expressions would have been far more complicated had one used $u_j = \dot{q}_j$, $j = 1,\ldots, n$. Substituting from Eqs. (4) and (3) in the following

$$\boldsymbol{v}^{P_j} = \boldsymbol{v}^C + \boldsymbol{\omega}^B \times \left[\boldsymbol{p}^{CP_0} + \sum_{i=1}^{3} q_{3j-3+i}\boldsymbol{b}_i\right] + \sum_{i=1}^{3} \dot{q}_{3j-3+i}\boldsymbol{b}_i \qquad (j = 1,\ldots, n) \tag{5}$$

leads to the equations

$$z_{ij} = p_i + q_{3j-3+i} \qquad (i = 1,2,3;\ j = 1,\ldots, n) \tag{6a}$$

$$\dot{q}_{3j-2} = u_{4+3j} - [u_4 + u_2 z_{3,j} - u_3 z_{2,j}] \qquad (j = 1,\ldots, n) \tag{6b}$$

$$\dot{q}_{3j-1} = u_{5+3j} - [u_5 + u_3 z_{1,j} - u_1 z_{3,j}] \qquad (j = 1,\ldots, n) \tag{6c}$$

$$\dot{q}_{3j} = u_{6+3j} - [u_6 + u_1 z_{2,j} - u_2 z_{1,j}] \qquad (j = 1,\ldots, n) \tag{6d}$$

Equating the derivative of the position vector from E to C with the velocity of C yields

$$\dot{q}_{3n+1} = u_4 - (u_2 q_{3n+3} - u_3 q_{3n+2}) \tag{7a}$$

$$\dot{q}_{3n+2} = u_5 - (u_3 q_{3n+1} - u_1 q_{3n+3}) \tag{7b}$$

$$\dot{q}_{3n+3} = u_6 - (u_1 q_{3n+2} - u_2 q_{3n+1}) \tag{7c}$$

Dynamical Equations

Equations (4) can be used to calculate the angular acceleration of B, the accelerations of C and P_j, the partial angular velocities[7] of B, and the partial velocities[7] of C and P_j. The

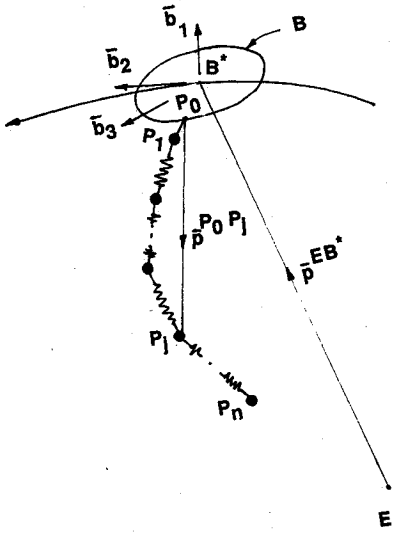

Fig. 1 Tethered payload model.

generalized inertia forces[7] can then be written as

$$F_1^* = -I_1\dot{u}_1 + (I_2 - I_3)u_2u_3 \tag{8a}$$

$$F_2^* = -I_2\dot{u}_2 + (I_3 - I_1)u_3u_1 \tag{8b}$$

$$F_3^* = -I_3\dot{u}_3 + (I_1 - I_2)u_1u_2 \tag{8c}$$

$$F_4^* = -m_B(\dot{u}_4 + u_2u_6 - u_3u_5) \tag{8d}$$

$$F_5^* = -m_B(\dot{u}_5 + u_3u_4 - u_1u_6) \tag{8e}$$

$$F_6^* = -m_B(\dot{u}_6 + u_1u_5 - u_2u_4) \tag{8f}$$

$$F_{4+3j}^* = -m_j(\dot{u}_{3j+4} + u_2u_{3j+6} - u_3u_{3j+5}) \quad (j = 1,\ldots, n) \tag{8g}$$

$$F_{5+3j}^* = -m_j(\dot{u}_{3j+5} + u_3u_{3j+4} - u_1u_{3j+6}) \quad (j = 1,\ldots, n) \tag{8h}$$

$$F_{6+3j}^* = -m_j(\dot{u}_{3j+6} + u_1u_{3j+5} - u_2u_{3j+4}) \quad (j = 1,\ldots, n) \tag{8i}$$

Generalized active forces[7] due to gravity are computed in the standard manner. The effects of gravitational moment on the spacecraft B are neglected.

$$F_i^g = 0 \qquad (i = 1,2,3) \tag{9a}$$

$$F_{3+i}^g = -\mu\, m_B q_{3n+i}\left(\sum_{j=1}^{3} q_{3n+j}^2\right)^{-3/2} \qquad (i = 1,2,3) \tag{9b}$$

$$z_{3+i,j} = q_{3n+i} + z_{i,j} \qquad (i = 1,2,3;\ j = 1,\ldots, n) \tag{9c}$$

$$z_{7,j} = \mu\, m_j\left(\sum_{i=1}^{3} z_{3+i}^2\right)^{-3/2} \qquad (j = 1,\ldots, n) \tag{9d}$$

$$F_{3+3j+i}^g = -z_{7,j}z_{3+i,j} \qquad (i = 1,2,3;\ j = 1,\ldots, n) \tag{9e}$$

Here μ is the universal gravitational constant times the mass of the Earth. Generalized forces due to the springs representing tether elasticity are formed, assuming that the tether cannot sustain compression and it has extensional stiffness k per segment of the tether.

$$z_{7+i,j} = q_{3j-3+i} - q_{3j-6+i} \qquad (i = 1,2,3;\ j = 2,\ldots, n) \tag{10a}$$

$$z_{11,j} = \left(\sum_{i=1}^{3} z_{7+i,j}^2\right)^{1/2} \qquad (j = 2,\ldots, n) \tag{10b}$$

$$z_{12,j} = z_{11,j} - L/n \qquad (j = 2,\ldots, n) \tag{10c}$$

or

$$z_{12,j} = 0 \quad \text{if} \quad z_{12,j} < 0 \qquad (j = 2,\ldots, n) \tag{10d}$$

$$z_{13,j} = k_j z_{12,j}/z_{11,j} \qquad (j = 2,\ldots, n) \tag{10e}$$

$$F_i^s = 0 \qquad (i = 1,\ldots, 9;\ n = 1) \tag{10f}$$

$$F_i^s = 0 \qquad (i = 1,\ldots, 6) \tag{10g}$$

$$F_{6+i}^s = z_{13,2}z_{7+i,2} \qquad (i = 1,2,3;\ n \geq 2) \tag{10h}$$

$$F_{9+i}^s = -F_{6+i}^s \qquad (i = 1,2,3;\ n = 2) \tag{10i}$$

$$F_{3+3j+i}^s = -z_{13,j}z_{7+i,j} + z_{13,j+1}z_{7+i,j+1} \qquad (i = 1,2,3;\ j = 2,\ldots, n-1) \tag{10j}$$

Generalized forces due to the interaction force needed for deployment are evaluated as follows:

$$F_i^c = \left[\tau\sum_{i=1}^{3} q_i\boldsymbol{b}_i\right]\cdot(\boldsymbol{v}_i^{P_0} - \boldsymbol{v}_i^{P_1}) \qquad (i = 1,\ldots, 6 + 3n) \tag{11a}$$

$$\tau = T\Big/\left(\sum_{i=1}^{3} q_i^2\right)^{1/2} \tag{11b}$$

where the quantity in parentheses in the first line is the negative of the partial velocity of separation of P_1 from P_0, which is obtained from the expression for the relative velocity of P_1 with respect to P_0. From Eq. (5) one finds

$$\boldsymbol{v}^{P_1} - \boldsymbol{v}^{P_0} = (u_2q_3 - u_3q_2 + \dot{q}_1)\boldsymbol{b}_1 + (u_3q_1 - u_1q_3 + \dot{q}_2)\boldsymbol{b}_2 + (u_1q_2 - u_2q_1 + \dot{q}_3)\boldsymbol{b}_3 \tag{12}$$

By using Eqs. (6) for $j = 1$ in Eq. (12), one gets

$$\boldsymbol{v}^{P_1} - \boldsymbol{v}^{P_0} = (u_7 - u_4 - u_2p_3 + u_3p_2)\boldsymbol{b}_1 + (u_8 - u_5 - u_3p_1 + u_1p_3)\boldsymbol{b}_2 + (u_9 - u_6 - u_1p_2 + u_2p_1)\boldsymbol{b}_3 \tag{13}$$

Now, the partial velocities needed in Eq. (11a) can be obtained by inspection of Eq. (13) and the generalized forces due to tether deployment force can be written:

$$y_1 = p_2q_3 - p_3q_2 \tag{14a}$$

$$y_2 = p_3q_1 - p_1q_3 \tag{14b}$$

$$y_3 = p_1q_2 - p_2q_1 \tag{14c}$$

$$F_i^c = y_i \qquad (i = 1,2,3) \tag{14d}$$

$$F_{3+i}^c = q_i \qquad (i = 1,2,3) \tag{14e}$$

$$F_{6+i}^c = -q_i \qquad (i = 1,2,3) \tag{14f}$$

Kane's dynamical equations[7] for the system are

$$F_i^* + F_i^g + F_i^s + F_i^c = 0 \qquad (i = 1,\ldots, 6 + 3n) \tag{15}$$

To these must be added an equation for deployment, which describes how the nominal length l of the tether changes with time. This can be written as the constraint condition

$$e = \sum_{i=1}^{3} q_i^2 - \left[l(t) - \frac{L(n-1)}{n}\right]^2 = 0 \tag{16}$$

To facilitate the solution of the differential-algebraic equations [Eqs. (15) and (16)], one replaces Eq. (16) with its twice-differentiated form, that is,

$$\ddot{e} = 2\left[\sum_{i=1}^{3}(q_i\ddot{q}_i + \dot{q}_i^2) - \dot{l}^2 - \dot{l}y_4\right] = 0 \tag{17a}$$

$$y_4 = l(t) - L(n-1)/n \tag{17b}$$

Now Eqs. (15) can be solved together with Eqs. (17). However, due to unavoidable errors in numerical integration, this scheme results in a violation of the constraint condition [Eq. (16)] with time. This situation is overcome by applying Baumgarte's[9] constraint stabilization procedure, which consists in writing the constraint equation as

$$\ddot{e} + k_v\dot{e} + k_pe = 0 \qquad (k_v > 0,\ k_p > 0) \tag{18}$$

where $\dot{e}$ is the time derivative of e in Eq. (16). Use of Eqs. (6) in the expression for $\ddot{e}$ in Eqs. (17) renders Eq. (18) into the form written in terms of the row matrix H and column matrix U as

$$H\dot{U}_1 = G \tag{19a}$$

$$H = [y_1\ y_1\ y_1\ q_1\ q_1\ q_1\ -q_1\ -q_1\ -q_1] \tag{19b}$$

$$U_1 = [u_1\ u_2\ u_3\ u_4\ u_5\ u_6\ u_7\ u_8\ u_9]^T \tag{19c}$$

$$G = -q_1(u_2\dot{q}_3 - u_3\dot{q}_2) - q_2(u_3\dot{q}_1 - u_1\dot{q}_3) \tag{19d}$$

$$-q_3(u_1\dot{q}_2 - u_2\dot{q}_1) - \dot{l}^2 + \sum_{i=1}^{3}\dot{q}_i^2 - \ddot{l}y_4 - k_v\dot{e} - k_p e \tag{19e}$$

It turns out[10] that Eqs. (15) can be written in the matrix form

$$M_1\dot{U}_1 = -C_1 + F_1 + H^T\tau \tag{20a}$$

$$M_2\dot{U}_2 = -C_2 + F_2 \tag{20b}$$

$$U_2 = [u_{10}\cdots u_{6+3n}]^T \qquad (n>2) \tag{20c}$$

where M_1, M_2, C_1, C_2, F_1, F_2 are defined as

$$\{F^*\} = \begin{bmatrix} M_1 & 0 \\ 0 & M_2 \end{bmatrix}\begin{Bmatrix}\dot{U}_1 \\ \dot{U}_2\end{Bmatrix} + \begin{Bmatrix}C_1 \\ C_2\end{Bmatrix} \tag{21a}$$

$$\{F^g + F^s\} = \begin{Bmatrix}F_1 \\ F_2\end{Bmatrix} \tag{21b}$$

where F^*, F^g, F^s are the column matrices whose elements are the left-hand sides of Eqs. (8–10), respectively. Eqs. (8) show that M_1, M_2 are diagonal matrices. Eqs. (19) and (20) permit the elimination of τ in Eqs. (20) and the development of explicit expressions for the dynamical equations, as follows:

$$y_4 = \sum_{i=1}^{3} y_i^2/I_i + \left(\sum_{i=1}^{3} q_i^2\right)(m_B + m_1)/(m_B m_1) \tag{22a}$$

$$\tau = \Bigg(G - \sum_{i=1}^{3}\{y_i[F_1(i) - C_1(i)]/I_i - \dot{q}_i[F_1(3+i) - C_1(3+i)]/m_B + q_i[F_1(6+i) - C_1(6+i)]/m_1\}\Bigg)\Big/ y_4 \tag{22b}$$

$$\dot{u}_i = [F_1(i) - C_1(i) + y_i\,\tau]/I_i \qquad (i = 1,2,3) \tag{22c}$$

$$\dot{u}_{3+i} = [F_1(3+i) - C_1(3+i) + q_i\,\tau]/m_B \quad (i = 1,2,3) \tag{22d}$$

$$\dot{u}_{6+i} = [F_1(6+i) - C_1(6+i) + q_i\,\tau]/m_1 \quad (i = 1,2,3) \tag{22e}$$

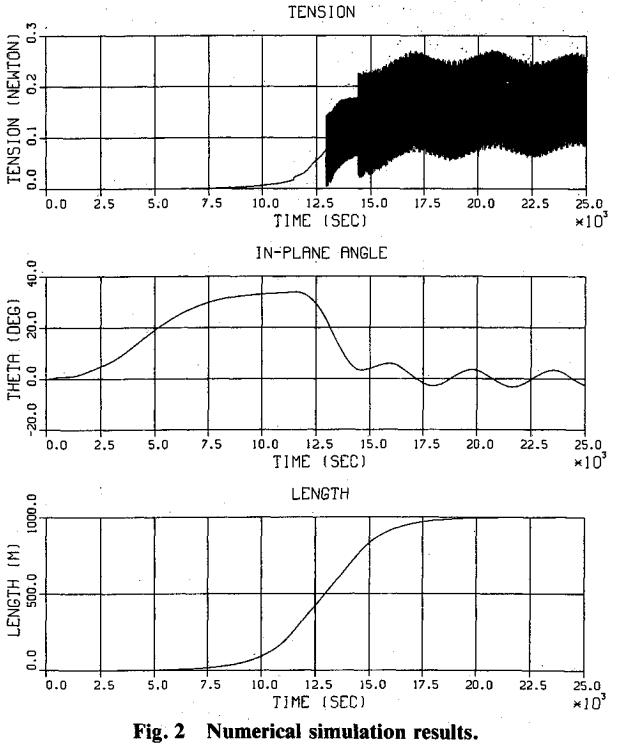

Fig. 2 Numerical simulation results.

$$\dot{u}_{3+3j+i} = [F_2(3j-6+i) - C_2(3j-6+i)]/m_j \qquad (i = 1,2,3;\ j = 2,\ldots,n) \tag{22f}$$

where $F_1(i)$, $C_1(i)$, $F_2(i)$, and $C_2(i)$ refer to the ith element in the column matrices F_1, C_1, F_2, and C_2, respectively. Note that the derivatives of the generalized speeds are uncoupled. This fact is primarily responsible for the speed of the numerical solution.

Numerical Simulation

Equations (6), (7), and (22) were numerically integrated for the following parameters: satellite orbit altitude 600 n.mi.; $m_B = 272$ kg, $I_1 = 41$ kg-m^2, $I_2 = I_3 = 542$ kg-m^2, tether attachment offset $p_1 = -1$ m, payload mass 45 kg, tether length $L = 1$ km, tether segment stiffness 373 N/m; constraint gains $k_v = 5.0$, $k_p = 6.32$. The tether mass was divided into five lumped masses from four tether segments when completely deployed. The method of updating the dynamical states by momentum conservation, as the number of particles increases by one during deployment, was done as per the description in Ref. 1 (p. 70). Figure 2 shows the plots for tether tension, in-plane angle for the line of sight to the payload, and tether deployed length which was prescribed via the rate control of Rheinforth[4]

$$\begin{aligned}\frac{dl}{dt} &= \alpha l, && 0<l<l_1\\ &= \alpha l_1, && l_1<l<l_2\\ &= \alpha l_1 - (L - l_2), && l_2<l<L\end{aligned} \tag{23}$$

where l_1 and l_2 are 250 and 750 m, respectively. The sharp increase in tension in the plot, as the number of particle masses deployed increases by one, appears to be a reflection of the modeling of the lumped mass deployment process. The dark band in the figure is due to plotting at 0.5-s interval tether tension arising from longitudinal oscillations at 1.36 Hz, added on the fluctuations due to in-plane libration of period 3750 s. The in-plane angle behavior, implying that the tether leads the orbiting body during deployment, has been reported in the literature.[1] Results shown are for a value of $\alpha = 0.7$ in Eq. (23). *Additional simulations show that the tether becomes slack for a faster initial rate of deployment, for example, for* $\alpha = 0.8$. Simulations of stationkeeping have also been done with this model setting, $dl/dt = 0$.

Conclusion

A method has been presented for *directly* incorporating a deployment rate control law with a lumped-mass tether model. The formulation is based on Kane's equations and treats the deployment rate specification as a motion constraint, but rather than eliminating one of the variables in terms of the others (which yields a set of equations uncoupled in the derivatives of the generalized speeds), it uses redundant coordinates and interaction forces to derive equations coupled in these derivatives. This device greatly reduces the computational time, while the choice of the generalized coordinates provides the necessary accuracy.

Acknowledgment

The author wishes to thank his colleague David Levinson for suggesting the choice of generalized speeds that resulted in substantial simplifications.

References

[1]Kallaghan, P. M., Arnold, D. A., Colombo, G., Grossi, M. D., Kirschner, L., and Orringer, O., "Study of the Dynamics of a Tethered Satellite System (Skyhook)," Smithsonian Astrophysical Observatory Report to NASA MSFC, Contract NAS8-32199, March 1978.

[2]Weber, R. and Brauchli, H., "Dynamics of a System of Two Satellites Connected by a Deployable and Extensible Tether of Finite Mass," Vols. I & II, ETH, Swiss Federal Inst. of Technology, Zurich, Switzerland, Rept. ESTEC Contract 2992/76/NL/AK(SC), 1978.

[3]Misra, A. K., and Modi, V. J., "A General Dynamical Model for the Space Shuttle Based Tethered Satellite System," *Advances in the Astronautical Sciences,* Vol. 40, Part II, 1979, pp. 537-557.

[4]Baker, W. P., Dunkin, J. A., Galaboff, A. J., Johnston, K. D., Kissel, R. R., Rheinfurth, M. H., and Seibel, M. P. P., "Tethered Subsatellite Study," NASA TM X-73314, March 1976.

[5]Liangdong, L., and Bainum, P. M., "Effect of Tether Flexibility on the Tethered Shuttle Subsatellite Stability and Control," *Journal of Guidance, Control, and Dynamics,* Vol. 12, No. 6, 1989, pp. 866-873.

[6]von Flotow, A. H., and Williamson, P. R., "Fast (3/4 Orbit) Deployment of a Tethered Satellite Pair to the Local Vertical," NASA/AIAA/PSN International Conf. on Tethers in Space, Arlington, VA, Sept. 17-19, 1986.

[7]Kane, T. R., and Levinson, D. A., *Dynamics,* McGraw-Hill, New York, 1985.

[8]Kane, T. R., and Levinson, D. A., "Formulation of Equations of Motion for Complex Spacecraft," *Journal of Guidance and Control,* Vol. 3, No. 2, 1980, pp. 99-112.

[9]Baumgarte, J., "Stabilization of Constraints and Integrals of Motion," *Computer Methods in Applied Mechanics and Engineering,* Vol. 1, 1972, pp. 1-16.

[10]Wang, J. T., and Huston, R. L., "Kane's Equations with Undetermined Multipliers—Application to Constrained Multibody Systems," *Journal of Applied Mechanics,* Vol. 54, June 1987, pp. 424-429.

Analysis of an Onboard Antenna Pointing Control System

Yoichi Kawakami,* Hiroshi Hojo,† and Masazumi Ueba†
Nippon Telegraph and Telephone Corporation
Radio Communication Systems Laboratories,
Yokosuka-shi, Kanagawa, Japan

Nomenclature

f_a = antenna drive control frequency
I_a = moment-of-inertia of antenna reflector
K_b = antenna drive ratio = antenna beam angle/reflector drive angle
q = modal coordinate of antenna structures
r = equivalent drive angle factor-reflector drive angle/reflector displacement
T_{ac} = antenna drive control torque
ζ_a = damping ratio of antenna support boom
θ_a = antenna drive angle
θ_p = antenna pointing error
ϕ_a, ϕ'_a = modal displacement and slope, respectively, of antenna support boom
ω_m = maximum satellite attitude rate
ω_n = eigenfrequency of antenna support boom

Introduction

IN the 1990s multibeam satellite communications systems must be developed to achieve larger transmission capacity. To establish these systems, large onboard antennas with high pointing accuracy are needed. In order to satisfy the requirements for high accuracy, new onboard control systems are being closely studied around the world.

In Japan, a field experiment of multibeam satellite communications is scheduled to be performed in conjunction with the sixth Japanese Engineering Test Satellite (ETS-VI), to be launched in 1992. ETS-VI is a two-ton class, three-axis stabilized geostationary satellite. The antenna pointing control systems on ETS-VI are now being designed. For this, the influence of dynamics on flexible structures must be considered. This paper describes significant system design parameters and relations between these values in the design of an onboard antenna pointing control system for ETS-VI.

System Configuration

The configuration of the onboard antenna pointing control system mounted on ETS-VI is shown in Fig. 1. An antenna drive control system (ADCS) is added to a conventional attitude control system (ACS). The ADCS consists of an rf sensor, an antenna pointing mechanism (APM), and antenna pointing control electronics (APE). The most important function of the ADCS is to point an antenna beam in the direction of a beacon transmitted from an Earth station and thereby minimize pointing errors residual in the antenna structures and the ACS. Since the rf sensor consists of a sensor feed and a reflector in common with the communications system, pointing errors of the reflector can be easily detected. An antenna beam can be shifted individually in orbit by rotating the subreflector with the APM.

Drive Methods

Two methods of antenna pointing control are currently used: a main-reflector drive and a subreflector drive. The main-reflector drive is electrically superior to the subreflector drive for yielding less antenna gain loss and lower sidelobe. This method, however, is mechanically inferior because of high inertial load and lower eigenfrequencies. Assuming that sinusoidal satellite attitude changes generate control errors in the antenna drive control, the pointing control error e can be represented as follows:

$$e = \omega_m / 2\pi f_a \tag{1}$$

Figure 2 gives the relationship between maximum permissible pointing control error as a function of control frequency for three satellite attitude rates. The control frequency is limited to about one-tenth of the eigenfrequency of the antenna reflector that is driven, to prevent the antenna structures from resonating. In our preliminary assessment of the structures, eigenfrequencies of the main reflector and the subreflector are about 2 and 10 Hz, respectively. As the maximum attitude rate of a two-ton class satellite is about 0.001 deg/s, the subreflector drive is preferable in order to achieve a pointing control accuracy of 0.001 deg.

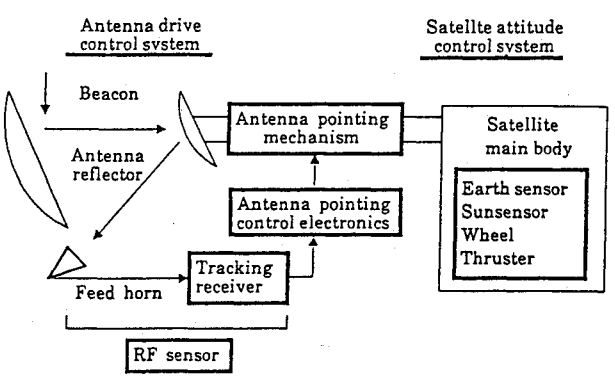

Fig. 1 Configuration of the antenna pointing control system.

Received Aug. 2, 1988; presented as Paper 88-4306 at the AIAA/AAS Astrodynamics Conference, Minneapolis, MN, Aug. 15-17, 1988; revision received March 31, 1989.

*Senior Research Engineer. Member AIAA.
†Research Engineer.